




TECHNICAL ARTICLE

Characterization and Upgrading of Low-grade Brahmaputra River Basin Ilmenite Concentrate: Exploring an Alternate Feedstock for Synthetic Rutile Preparation

MD. SHOHEL RANA ^{1,5} MADHU SUDAN SAHA,²
PRADIP KUMAR BISWAS,¹ MD SHAMS SHAHRIAR,^{1,4}
FIROZ AHMED,³ and MOHAMMAD NAZIM ZAMAN¹

1.—Institute of Mining, Mineralogy and Metallurgy (IMMM), Bangladesh Council of Scientific and Industrial Research (BCSIR), Joypurhat 5900, Bangladesh. 2.—Leather Research Institute (LRI), Bangladesh Council of Scientific and Industrial Research (BCSIR), Dhaka 1350, Bangladesh. 3.—BCSIR Laboratories Rajshahi, Bangladesh Council of Scientific and Industrial Research (BCSIR), Rajshahi 6206, Bangladesh. 4.—School of Earth and Environmental Sciences, The University of Queensland, St Lucia, QLD 4072, Australia. 5.—e-mail: shohelrana@bcsir.gov.bd

This research focuses on characterizing river basin ilmenite and upgrading it to synthetic rutile through direct hydrochloric acid leaching. The ilmenite was fractionated from heavy mineral concentrates by physical separation, which were collected from the transboundary Brahmaputra River basin sandbars in Bangladesh. The ilmenite and prepared titanium products were characterized by wavelength dispersive x-ray fluorescence, grain size analysis, x-ray diffraction, optical and scanning electron microscopy, and Raman spectroscopy. The river basin ilmenite concentrate is low grade and contains 27.02% TiO_2 and 60.62% Fe_2O_3^t , composed of ilmenite, hemo-ilmenite, ilmenohematite, and some locked grains of gangue minerals. The titanium product prepared from river basin ilmenite by direct hydrometallurgical processing showed 95.61% TiO_2 , 3.81% Fe_2O_3^t , and 0.58% other oxides, and corresponds to a complete rutile phase. This synthetic rutile also exhibited a porous structure, crushed crystallites, and a particle size of $< 0.5 \mu\text{m}$. Except for the Fe_2O_3^t content, which might be reduced by chlorination, all the attributes of the synthetic rutile meet the requirements for industrial use. This could make river basin ilmenite a viable alternative to conventional ilmenite feedstock from beach placers or massive crystalline ores.

INTRODUCTION

Ilmenite and other titanium minerals have undergone chemical modification to become synthetic rutile (TiO_2), which has many fields of application due to its distinctive properties, e.g., being highly refractive and extra white and having greater chemical stability.^{1–3} Synthetic rutile is used as a raw material in the manufacture of paints, plastic, coatings, welding electrodes, ceramics, paper, paperboard, and printing inks.^{2,4–6} The global

demand for titanium minerals is primarily driven by the need for white TiO_2 pigment, with approximately 90–95% of titanium mineral production used for this purpose.^{1,7} According to the report of USGS mineral commodity summaries, the estimated world reserve of ilmenite is 650 Mt, whereas rutile is only 49 Mt for the year 2022.⁷ Due to the shortage of rutile in nature, ilmenite is mined higher than rutile to meet market demand. Furthermore, the market price of synthetic rutile is four to five times that of ilmenite.⁸ Accordingly, ilmenite is being preferred as a substitute for natural rutile because of its availability, higher demand, and lower cost. The aforesaid phenomenon urges the upgrading of ilmenite, which is the main feed

(Received April 18, 2023; accepted September 18, 2023;
published online October 16, 2023)

mineral in the production of synthetic rutile, among other Ti-bearing minerals, e.g., rutile, leucosene, titanomagnetite, etc.^{2,6} Approximately 90% of the world's demand for titanium is met by ilmenite.⁷ This demand is significantly motivating researchers to upgrade ilmenite to titanium slag or synthetic rutile.^{9–12} The impurity levels in ilmenite, including Si, Al, Mg, Cr, and Mn, can affect its market value,¹³ further driving the need for upgrading. Commercially, synthetic rutile (TiO_2) manufacturing uses one of the following processes: pre-treatment process (smelting or reduction-oxidation followed by leaching), direct hydrometallurgical process, sulfate process, and chloride process worldwide.^{1,2,14} The sulfuric acid process is highly polluting; on the other hand, the chloride process is more eco-friendly and generates less waste.^{9,14} Again, the direct hydrometallurgical process is a simple chemical process because of its easy handling, convenience, and fewer stages. Through digestion in strong HCl acid, low-grade ilmenite is transformed into TiO_2 pigment in the direct hydrometallurgical process.⁹

Several studies have reported the preparation of high-quality synthetic rutile (> 89% TiO_2) from either ilmenite ore or beach placer concentrates using a hydrochloric (HCl) acid leaching process.^{4,10–12,15,16} The Magpie process, introduced by Habashi et al.,⁹ allows for the synthesis of high-grade synthetic rutile (more than 95% TiO_2) from low-grade ilmenite (10–12% TiO_2) ore sourced from massive deposits in Quebec Province, Canada. El-Hazek et al.⁴ studied mainly the optimum dissolution conditions of the ilmenite concentrate in HCl, in which the feed material was collected from the Mediterranean beach of Rosetta, Egypt. In addition, the other authors, e.g., Lasheen,¹⁰ Li et al.,¹¹ Mahmoud et al.,¹² Sarker et al.,¹⁵ and Sasikumar et al.,¹⁶ also successfully evaluated the synthetic rutile production either from beach sand placers or massive ore from Rosetta beach (Egypt), Panzihua massive ore (China), Abu Ghalaga massive ore (Egypt), Cox's Bazar beach (Bangladesh), and Orissa beach sand (India), respectively. Earlier studies on the preparation of synthetic rutile from Bangladesh ilmenite derived from Cox's Bazar beach sand through the reduction-leach route were conducted with promising outcomes.^{15,17,18} Typically, titanium minerals are mined from ore bodies of massive crystalline rocks, either weathered or intact, as well as unconsolidated shoreline beach placer deposits worldwide, rather than fluvial river basin sources.¹⁹ Accordingly, there is a great scope of research on using feed materials like ilmenite collected from river basin placer deposits for synthetic rutile preparation.

There are numerous methods, either pyrometallurgical or hydrometallurgical, or combinations of both, to convert ilmenite to a titanium product with > 90% (TiO_2) purity, e.g., the Becher process, Benilite process, Austpac process, alkaline roasting and leaching, and direct acid leaching.^{2,6,20} Direct

hydrometallurgical leaching of ilmenite has recently gained attention, and this process, as opposed to electro-chemical and thermo-chemical processes, is beneficial in processing huge amounts of ilmenite ores because of its low energy consumption, fewer processing stages, and the manufacture of adequately high-quality pigment-grade titanium dioxide products for a wide range of applications.^{2,6,21} Besides, numerous scholars have studied the impact of mechanical activation on the dissolution rate of ilmenite.^{22–25} They mentioned that mechanical activation speeds up the rate of dissolution of ilmenite by enhancing its chemical reactivity. In this way, acid leaching by HCl of mechanically activated ilmenite is a potential route for upgrading to synthetic rutile.

Researchers studied crystalline ilmenite ore or beach placer ilmenite feed material from different parts of the world for synthetic rutile preparation that contains 40–65% TiO_2 .^{2,4,6,10–12,16,26,27} Contrarily, the ilmenite from the Brahmaputra River basin sand has about 24.3–30.4% TiO_2 with 61.9–69.7% Fe_2O_3 , 3.96–4.82% SiO_2 , 1.88–1.43% Al_2O_3 , 0.74–1% CaO, and < 2.38% other oxides,^{19,28} making it lower grade than beach placer ilmenite.^{14,24,26} Based on the mineral's chemical composition, Rahman et al.¹⁹ suggested using the sulfate route for pigment production from the ilmenite-rich component of the Brahmaputra River.

The transboundary Ganges-Brahmaputra-Meghna (GBM) river systems carry the world's greatest sediment load, estimated at about 1.0–2.4 billion tons annually,^{29,30} which is constantly replenished from the catchment area of these river systems. Large-scale mineral sand deposits found in the GBM river basin have sparked significant interest as a potential heavy mineral resource. The bulk sand from the Brahmaputra, Ganges (Padma), Meghna, and Tista Rivers contains about 10.73 wt.%, 7.0 wt.%, 9.0 wt.%, and 10.99 wt.% of total heavy minerals (THM), respectively.^{28,31–33} Ilmenite is a key component of THM, which can make it an attractive alternative source to synthetic rutile feedstock.¹⁹ Generally, synthetic rutile production is well studied using ilmenite found in beach placers or massive crystalline ores.^{2,4,6,10–12,16,26,27} However, no research has been reported on the river basin ilmenite upgrade to synthetic rutile to date. This research gap on fluvial river basin ilmenite greatly encouraged the present work, which will open up new avenues in river basin mineral resource processing. Therefore, the aim of this research is to characterize the Brahmaputra River basin ilmenite (FeTiO_3) concentrate, and an attempt has been made to upgrade it to synthetic rutile (TiO_2) using direct hydrochloric acid leaching.

LOCATION AND SAMPLING METHOD

The samples of heavy mineral assemblages were collected from the clastic sediments of the Brahmaputra River basin, Kurigram, Bangladesh (Fig. 1).

The sampling area is located in the northernmost part of Bangladesh, close to the Bangladesh-India border. The sand-bedded, braided Brahmaputra River has a total length of 2900 km from its origin in the Mansarovar Lake region near Mount Kailash in the Himalayas.³⁴ The total catchment area of the Brahmaputra River is 540,000 km², spread across the countries of Tibet (China), India, Bhutan, and Bangladesh.³⁵ It is the 15th longest river in the world and the 9th largest by discharge.³⁶ In the Bangladesh part, it has individual channels that are 2–3 km wide, and it has a lateral span of around 15 km.³⁷ Valuable heavy minerals, such as magnetite, ilmenite, garnet, titanite, rutile, and zircon, as well as other heavy mineral assemblages, such as amphibole, epidote, sillimanite, kyanite, etc., are potentially present in the Brahmaputra River sands.^{28,38,39} From a geomorphological perspective,

the Brahmaputra River has numerous recently developed in-channel river bars, which is typical of this type of braided river.³⁷

The enormous amounts of heavy mineral (HM) deposits were concentrated scattered throughout the sandbar of the braided river by the action of flowing water from upstream during the dry season. The HM samples were taken during the dry period and collected by hand auger from sandbars up to a maximum depth of 1 m. The longitudinal spacing between each of the sample locations was approximately 1.5–2 km, based on the occurrence of HM deposits. A total of 20 samples were collected for the current study (Fig. 1). Like other placer deposits, the HM assemblages were loose, unconsolidated, and almost free of clay-sized particles. To get a representative composite HM sample of the whole channel, the collected HM samples were mixed

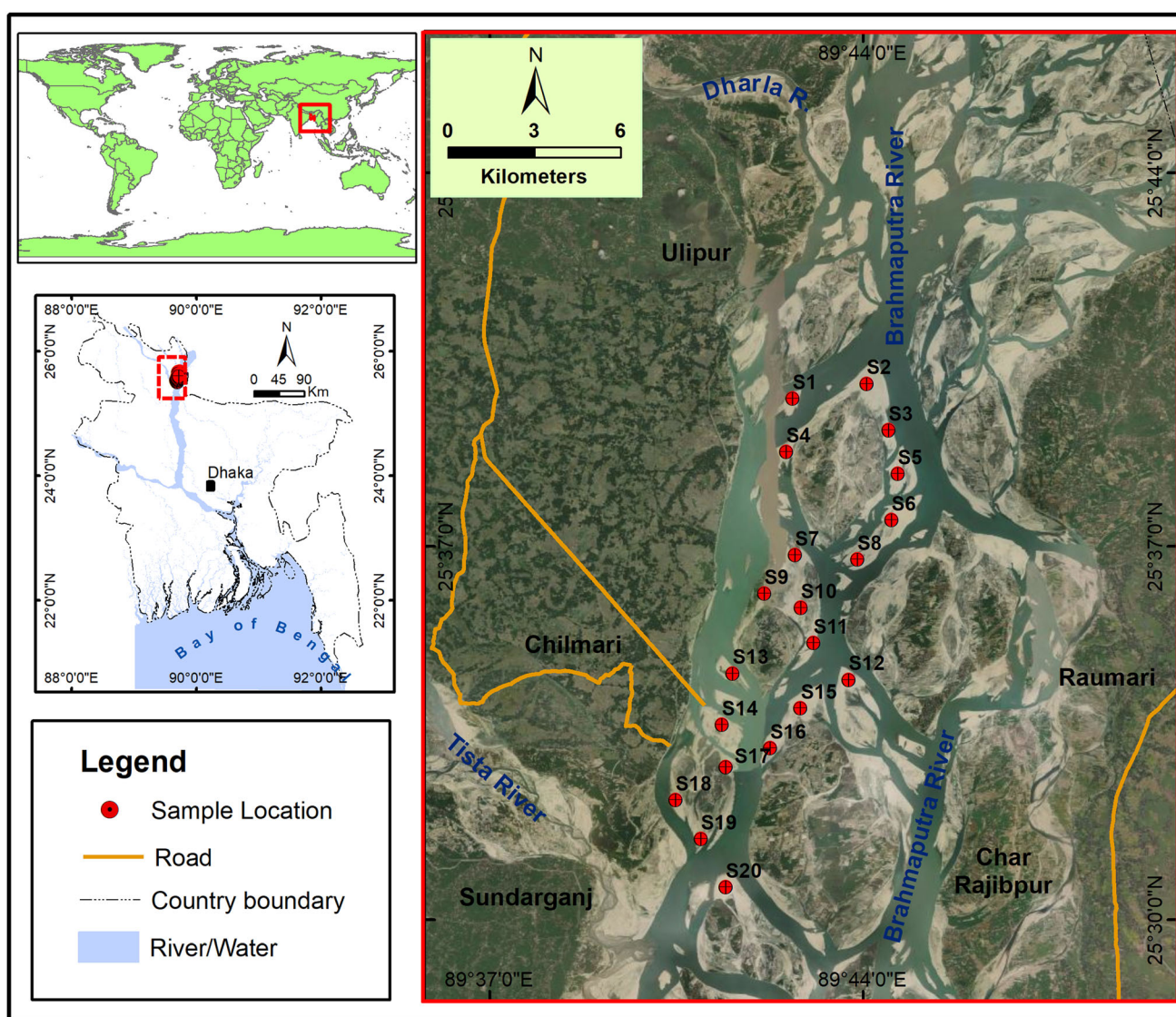


Fig. 1. Location map of sampling in the Brahmaputra River basin, Kurigram, Bangladesh (adapted from Google Earth, <https://earth.google.com/>).

before the physical separation of ilmenite. Finally, the mixed HM assemblages were passed through steps of physical separation.

MATERIALS AND METHODS

Physical Separation of Ilmenite

The physical separation technique is crucial for obtaining a high-quality ilmenite concentrate, which is a valuable source of titanium dioxide (TiO_2) for various industrial applications. Ilmenite concentrate was obtained by physical separation processes from the collected river basin HM sand samples of the Brahmaputra River in Bangladesh. Initially, a shaking table (density separation method) was used to separate heavy minerals from light minerals and generate bulk heavy mineral concentrate (HMC). Then, a weak hand magnet was used to fractionate magnetite from HMC. As ilmenite has both magnetic and conductive properties, at this stage it was further separated from remaining non-ilmenite minerals (garnet, rutile, zircon, aluminosilicates, etc.) using a high-intensity induced roll magnetic separator (IRMS) and an electrostatic plate separator (ESPS), respectively.⁴⁰ The recovered ilmenite from this fractionation process was further analyzed to determine its mineralogical and chemical composition and subjected to a chemical experiment.

Analytical Procedure

The chemical composition of the specimens was determined using a wavelength dispersive x-ray fluorescence (WDXRF) spectrometer (Rigaku ZSX Primus, Japan) according to the procedure of Norrish and Hutton.⁴¹ The crystalline phase identification of these materials was carried out using x-ray diffraction (XRD) analysis (Panalytical XPERT-PRO (PW3040/60), The Netherlands) with a continuous scanning speed of $2^\circ 2\theta/\text{min}$. An x-ray pattern ($10\text{--}70^\circ 2\theta$) was obtained from the dry powdered samples following the procedures of Lindholm.⁴² Raman spectroscopy of the synthetic rutile was executed at room temperature using a Raman spectrometer (Horiba MacroRam, Japan) with a 785-nm diode laser as the excitation source. To analyze the grain size distribution (GSD) of ilmenite concentrate, mechanical sieving was used based on ASTM D422.⁴³ The grain size of the mechanically activated ilmenite was determined by the laser diffraction method using a particle size analyzer (Microtrac S-3500, USA). Microscopic-polished section examination was performed by Axio Imager.M2m, Carl Zeiss, Germany, to depict the alteration, exsolutions, grain shapes, fracturing, etc. The field-emission scanning electron microscope (FESEM) imaging was completed using a ZEISS Sigma 300 (Gemini), UK, to study the surface morphology of the samples.

Experimental Procedure

The ilmenite concentrate was mechanically activated using a planetary ball mill (*Retsch PM 200, Germany*) with a spin rate of 250 rpm, sample/ball ratio of 1:2 (v/v), and milling time of 25 min. The milled samples of 20 g were leached in a 250-ml three-necked glass reactor equipped with a reflux condenser. A thermometer was used to measure the temperature of the reaction. A silicone oil bath was used for a thermostatically controlled reaction, i.e., the temperatures were equally distributed over the reactor. In the reactor, mechanically activated ilmenite was directly mixed with hydrochloric acid (37% or 12.08 M). The variable acid content was used during leaching based on the stoichiometric ratio of HCl acid and ilmenite (FeTiO_3) reaction as 4:1 followed by 5:1 and 6:1. The other leaching parameters, e.g., leaching temperature, leaching time, and stirring speed, were optimized based on the systematic laboratory trial-and-error method on multiple leaching tests. From the rigorous trial-and-error method, the leaching conditions were set using concentrated HCl at $75 \pm 5^\circ\text{C}$ for 3 h, stirring at 250 rpm and ambient pressure with variable acid-to-ilmenite ratios (v/w) (4:1, 5:1, and 6:1).

A two-stage leaching process was performed to recover synthetic rutile from low-grade river basin ilmenite concentrate (Fig. 2). At the end of each leaching, the slurry was filtered and washed with deionized water. The spent liquor was collected after the first leaching stage, and the residue was subjected to the second stage of leaching. After second-stage leaching, the residue was discarded as it was composed of unreacted silicate gangue minerals.⁹ The spent liquor from the first and second stages of leaching was boiled at $70\text{--}80^\circ\text{C}$. This

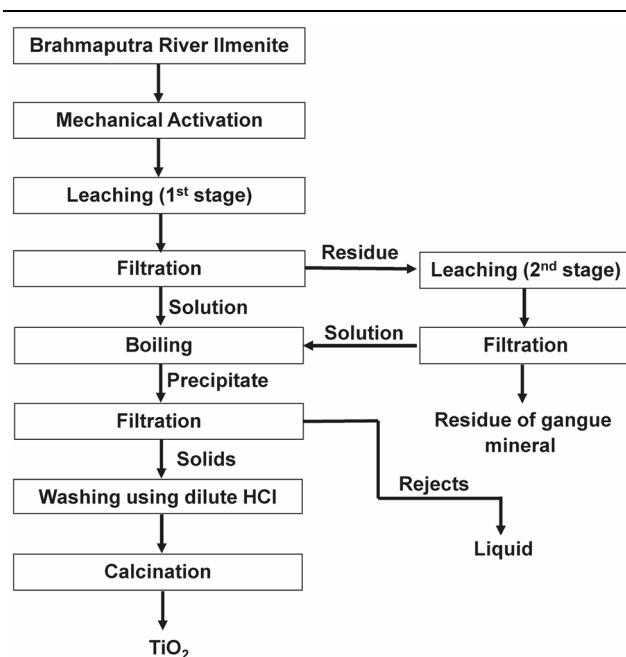
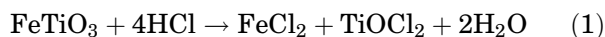


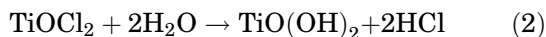
Fig. 2. Flowsheet for the preparation of titanium products.

treatment framework was followed during the leaching of different acid-to-ilmenite ratios (v/w) of 4:5, 5:1, and 6:1, respectively. Subsequently, the spent liquor from the first and second stages of leaching was boiled at 70–80°C. After optimum boiling, titanyl oxyhydroxide [TiO(OH)₂] was obtained as a precipitate, where iron remains in solution and reacts with the Cl⁻ ion to form FeCl₂. Finally, filtration of the [TiO(OH)₂] from solution was carried out and subsequently calcination (850°C for 1.5 h) of titanyl oxyhydroxide leaving the titanium dioxide (TiO₂) powder. A simplified flowsheet of the extraction of titanium products from mechanically activated Brahmaputra River basin ilmenite using direct HCl acid leaching is depicted in Fig. 2. In summary, the reaction mechanism is explained by the following Eqs. 1–4.

During leaching, the ilmenite (FeTiO₃) reacts with hydrochloric acid (HCl) to produce ferrous chloride (FeCl₂), titanium oxychloride (TiOCl₂), and water (H₂O).



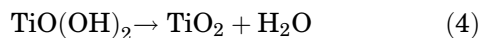
Subsequently, titanyl oxyhydroxide [TiO(OH)₂] and hydrochloric acid (HCl) are formed as a result of the reaction between titanium oxychloride (TiOCl₂) and water (H₂O).



The obtained solution after leaching was boiled at 70–80°C, which resulted in the precipitation of titanyl oxyhydroxide [TiO(OH)₂] from the hydrochloric acid solution.



After cooling the solution, the titanyl oxyhydroxide [TiO(OH)₂] was filtered and dried, and then subjected to calcination, where it transformed into titanium dioxide (TiO₂) powder, and the inherent water (H₂O) was vaporized.



RESULTS AND DISCUSSIONS

Characterization of Ilmenite Concentrate

The chemical compositions of the Brahmaputra River ilmenite concentrate showed 27.02% TiO₂ and 60.62% Fe₂O₃^t, with other oxides as impurities of 12.36% (Table I). The higher Fe₂O₃^t content (60.62%) of the analyzed concentrate suggests contamination by titano-magnetite, titano-hematite, hemo-ilmenite, and ilmeno-hematite particles.^{19,20} The existence of silica (SiO₂ 5.89%) as an impurity in the Brahmaputra River ilmenite indicates the presence of silicate minerals, which are resistant to dissolution in HCl acid.⁴⁴ The availability of comparatively high levels of oxides of Si, Al, Fe, Ca, Mg,

Cr, and Mn in the ilmenite concentrate indicates that it is less pure and reduces its market value.⁴⁵ The TiO₂ percentage of ilmenite sourced from river basins is relatively low (27.02% TiO₂), and higher amounts of other impurities are present than in the beach or crystalline ore of ilmenite,^{4,10,14,19,26,27} which indicates the raw material is low-grade. On the other hand, the beach ilmenite and massive ilmenite ore feedstock is usually medium-to-high grade and contains 40–65% TiO₂ compared to the analyzed river basin ilmenite concentrate.^{2,4,10–12,15,16,26,27,46} Besides, the beach placer ilmenite or crystalline ilmenite ore has fewer impurities (Si, Al, Fe, Ca, Mg, Cr, Mn, etc.) than the river basin ilmenite (Table I), is a common source of feed materials for TiO₂ synthesis, and is commercially used as a feedstock.^{2,20,26} The impurity level of the river basin ilmenite is greater than in the beach placers (Table I), revealing probable facts related to mineral liberation and gangue mineral properties that responded differentially during separation.¹⁹ In line with the discussion, the composition of low-grade ilmenite concentrate from the Brahmaputra River basin makes it difficult to use in industry for pigment production and requires further analysis and understanding of the intended use for a particular application.

The grain size distribution of the ilmenite concentrate is shown in Fig. 3. The ilmenite concentrate has a narrow size distribution, and about 93% of the ilmenite has grain size ranging between – 250 μm and + 90 μm with an average passing size (d₅₀) of 168 μm (Fig. 3). Sasikumar et al.¹⁶ studied the ilmenite from Orissa beach sand, India, whose size range varies between 100 μm and 500 μm, and mentioned that the dissolution rate of both iron and titanium using sulfuric acid was significantly enhanced by mechanical activation. The size range of Brahmaputra River basin ilmenite is consistent with the findings of Sasikumar et al.¹⁶ and suggests that mechanical activation would enhance further chemical reactions. Moreover, the uniformity coefficient (C_U) and coefficient of curvature (C_C) values are 1.59 and 0.97, respectively, which indicate poorly graded ilmenite concentrate.⁴⁷ This implies a small range of variation in grain sizes in Brahmaputra River basin ilmenite.

The raw material, ilmenite concentrate, is mineralogically composed of ilmenite phases with less hematite and minor quartz and rutile, as determined by the peak positions (°2θ) and d-spacing (Å) of the x-ray diffraction pattern (Fig. 4). Ilmenite is the primary mineral constituent of the analyzed specimen, and the peak positions of this mineral were well matched with the standard ICDD database (#00-029-0733). The dominant secondary mineral, i.e., hematite, was identified in the XRD pattern, which showed similarities with the standard ICDD card (#00-33-0664). The mineralogical impurities such as hematite, quartz, and rutile in the river basin ilmenite concentrate suggest a lower

Table I. Chemical composition (wt.%) of ilmenite concentrate from the Brahmaputra River basin and other sources

Oxides (wt.%)	Brahmaputra River basin ilmenite concentrate	Beach ilmenite from Orissa, India ¹⁶	Beach ilmenite from Murray Basin, Australia ⁴⁶	Rosetta beach ilmenite, Egypt ¹⁰	Ilmenite ore from Abu Ghalaga, Egypt ²⁷
MgO	0.85	0.72	0.67	0.80	3.38
Al ₂ O ₃	1.97	0.45	0.55	0.80	1.10
SiO ₂	5.89	0.70	0.76	0.55	1.97
P ₂ O ₅	0.12	–	0.01	0.26	0.05
CaO	1.22	0.05	0.04	0.44	0.33
TiO ₂	27.02	50.55	50.40	46.69	40.91
Cr ₂ O ₃	0.56	0.05	0.09	0.29	0.071
MnO	0.96	0.54	0.61	1.15	0.25
Fe ₂ O ₃ [†]	60.62	46.50	46.20	48.40	51.91
Nb ₂ O ₅	0.03	–	0.11	–	–
V ₂ O ₅	–	0.23	0.28	0.178	–

[†]Fe₂O₃[†] = Total of FeO + Fe₂O₃.

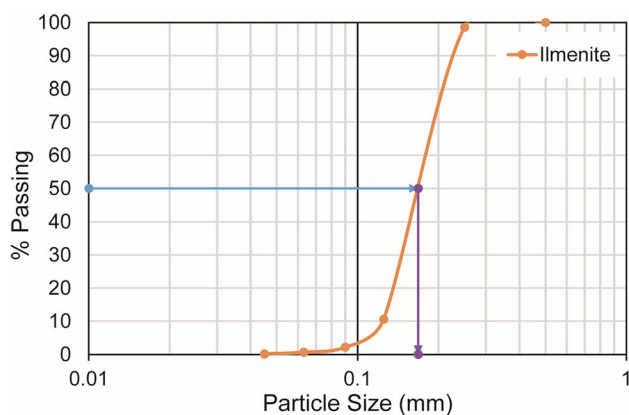


Fig. 3. Grain size distribution curve of river ilmenite concentrate.

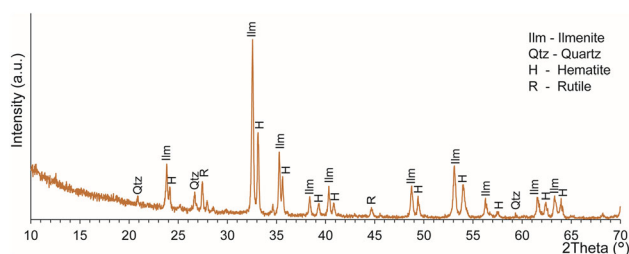


Fig. 4. X-ray diffraction pattern of ilmenite concentrate.

degree of liberation, chemical weathering, sorting, reworking, etc.⁴⁵ The mineralogical compositions are well consistent with the findings of Mehdilo and Irannajad¹⁴ and Rahman et al.¹⁹ Besides, the XRD result is compatible with the chemical composition data, i.e., the presence of hematite and quartz degrades the quality of ilmenite (TiO₂ = 27.02%).

Back-scattered electron (BSE) images were taken using FESEM, and the photomicrograph of the ore slide of ilmenite concentrate was obtained by a

reflected light microscope (*Axio Imager.M2m*) and is shown in Fig. 5. The BSE image exhibits a sub-angular to sub-rounded grain shape (Fig. 5a). Referring to Fig. 5, the ilmenite concentrate contains liberated ilmenite grains, hemo-ilmenite, ilmeno-hematite, and some locked grains of gangue minerals as inclusions.^{19,20} The BSE micrograph in Fig. 5a shows the elongated shape of the ilmenite grain. Some of the grain surface in Fig. 5b is marked by numerous surface pits and veins. This is an indication of alteration and suggests atomic relocation from the lattice of the crystalline structure. Both exsolution bodies of hematite in the ilmenite grains and ilmenite exsolutions in the hematite grains are present (Fig. 5). The exsolution-oxidation or oxy-exsolution processes might be the causes of the ilmenite or hematite exsolution phenomenon in the Brahmaputra River ilmenite concentrate.^{19,48} The elongated hematite lamellae were oriented in a regular texture within the ilmenite grain. Additionally, there are significant variations in exsolution distribution between grains. The texture indicates that fluvial ilmenite is moderately exsolved (Fig. 5), and the chemical composition (Table I) supports this assessment. Micro-fracture within the grains of ilmenite concentrate has also been seen. The gangue minerals inclusion, hematite exsolutions (Fig. 5), and presence of Si, Al, Mg, and Mn (Table I) tended to deteriorate the quality of ilmenite concentrate as pigment production feed.¹⁴ The mineralogical characteristics of the photomicrographs (Fig. 5) were strongly comparable with the XRD and chemical composition results (Table I and Fig. 4) of the analyzed specimen.

Mechanical activation of ilmenite concentrate has been accomplished for the purposes of decreasing crystallite size, increasing specific surface area and chemical reactivity, and enhancing the dissolution

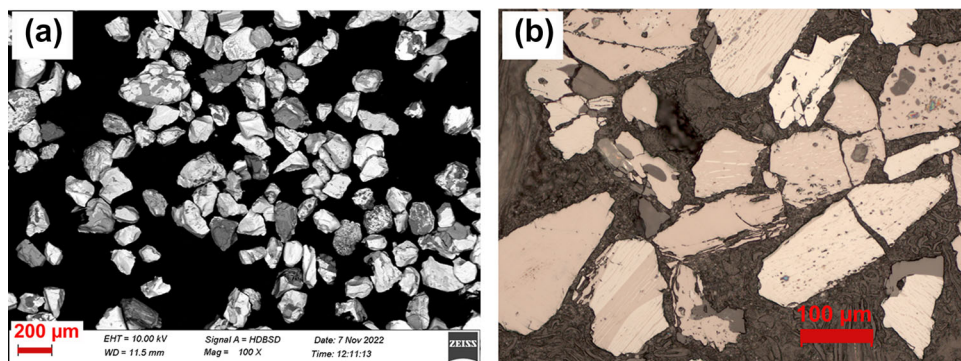


Fig. 5. (a) Back-scattered electron (BSE) image of ilmenite concentrate and (b) cross-sectional image of ilmenite concentrate from an ore microscope. (Note: the dark bands represent ilmenite, the bright bands are made up of hematite, and the pits are inclusions).

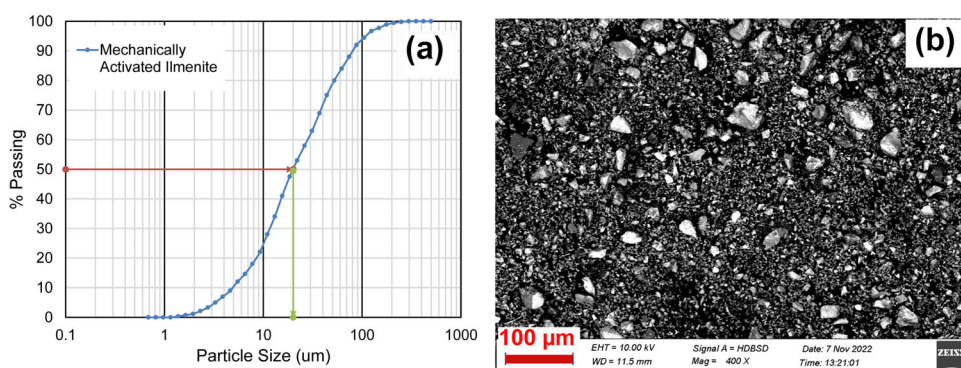


Fig. 6. (a) Grain size distribution curve of mechanically activated ilmenite and (b) back-scattered electron (BSE) microphotograph of mechanically activated ilmenite.

of Ti and Fe during leaching.^{11,16,24} Also, the ilmenite particle's internal structure was disrupted during the mechanical activation process, resulting in flaws, fissures, and exposed reactive surfaces. The mechanically activated ilmenite had an average size (d_{50}) of 20.09 μm (Fig. 6a), whereas the size of the river basin ilmenite was 168 μm (d_{50}). This reduction in size can significantly impact the chemical reaction by enhancing chemical reactivity and the dissolution of particles.^{11,16,24} The FESEM photomicrograph in the backscattered electron imaging of a milled specimen exhibited the formation of irregular angular to sub-angular grains due to the breakdown of the primary particles (Fig. 6b). This is a direct result of the mechanical forces applied during milling, which lead to the fragmentation and breakdown of the primary ilmenite particles. This mechanically activated ilmenite will go through further leaching experiments for the extraction of the titanium product.

Ilmenite Upgrading

In this study, an attempt has been made to determine the outcomes of river basin ilmenite conversion to synthetic rutile. For this reason, the low-grade river basin ilmenite concentrate of the

Brahmaputra River was upgraded to a titanium (TiO_2) product by direct HCl acid leaching. The prepared product was characterized based on chemical composition, XRD and Raman analysis, and FESEM. Before going to the leaching process, the granular river basin ilmenite samples ($-250 \mu\text{m}$ to $+90 \mu\text{m}$ in size) were ground by a planetary ball mill using a method of mechanical activation. The mechanically activated river basin ilmenite concentrate was processed through leaching, filtration, boiling, and calcination to obtain the upgraded titanium product (TiO_2), which was characterized later.

Characterization of Prepared Titanium (TiO_2) Product

The laboratory leaching experiments of mechanically activated river basin ilmenite concentrate were performed in a variable acid-to-ilmenite ratio for the preparation of titanium-based products, e.g., synthetic rutile (TiO_2), while the leaching temperature, time, and stirring speed were kept fixed at $75 \pm 5^\circ\text{C}$, 3 h, and 250 rpm, respectively, with ambient pressure. The three different acid-to-ilmenite ratios (v/w) were 4:1, 5:1, and 6:1, and the products obtained under these different leaching

conditions were denoted as R-1, R-2, and R-3, respectively. The chemical analysis results obtained by WDXRF of prepared products from river basin ilmenite concentrate are given in Table II. Chemically, the final product R-1 was composed of 86.27% TiO₂ and 13.19% Fe₂O₃^t, whereas R-2 and R-3 specimens were composed of 95.61% TiO₂, 3.81% Fe₂O₃^t, and 90.14% TiO₂, 9.20% Fe₂O₃^t, respectively, with traces of other oxides (Table II).

The products R-1 and R-3 contain less TiO₂ (86.27–90.14%) with high iron oxides (Fe₂O₃ 13.19–9.2%) than R-2 (95.61% TiO₂ and 3.81% Fe₂O₃^t), suggesting further treatment before use in industry for the manufacture of pigment. This iron content of R-1, R-2, and R-3 specimens might be removed by the selective chlorination process,⁴⁹ washing with dilute acid, and drying. Conversely, the prepared products have a minor amount (0.49–0.64%) of Al₂O₃, SiO₂, P₂O₅, CaO, and Nb₂O₅ and the absence of MnO and Cr₂O₃ coloring agents, making them compatible for white pigment manufacturing by chlorination.²⁷

However, the titanium product prepared by using acid-to-ilmenite ratios (v/w) of 4:1 and 6:1 (R-1 and R-3) has lower TiO₂ purity and higher impurities than product R-2 (acid-to-ilmenite ratio (v/w) of 5:1). Furthermore, the specimen R-2 has the highest TiO₂ content (95.61%) and can be designated as high-grade in terms of TiO₂ purity. This high TiO₂ content in the extracted product is consistent with the findings of Mehdilo and Irannajad,¹⁴ Lasheen,¹⁰ Li et al.,¹¹ Mahmoud et al.,¹² Sarker et al.,¹⁵ Jung et al.,⁴⁹ and Shahien et al.²⁷ on the production of synthetic rutile. Thus, the product R-2 is considered an excellent titanium-based product in this current

study compared to R-1 and R-3, which were prepared at an acid-to-ilmenite ratio of 5:1 (v/w), 75 ± 5°C leaching temperature, 3 h leaching time, and 250 rpm stirring speed.

Compared to the synthetic rutile preparation from either beach ilmenite or ilmenite ore (Table II), the TiO₂ content of the R-2 specimen (95.61%) is strongly consistent with the findings of synthetic rutile (95.92–97.30% TiO₂) prepared from beach ilmenite of Murray Basin, Australia, and ilmenite ore of Abu Ghalaga, Egypt,^{27,46} but higher than synthetic rutile (89.00% TiO₂) manufactured from Rosetta beach ilmenite, Egypt,¹⁰ and Tronox, Western Australia (TiO₂ 92.00%).^{20,50} The amount of other oxides (Si, Ca, P, and Nb) in the prepared R-2 product is rational except for total Fe₂O₃, which is slightly higher than synthetic rutile from Murray Basin, Abu Ghalaga, and Tronox ilmenite^{20,27,46,50} but lower than synthetic rutile from Rosetta Beach ilmenite.¹⁰ The chemical framework of the R-2 product suggests that the present river basin ilmenite is a promising new feedstock for synthetic rutile preparation.

To know the phases of the prepared products, XRD analysis was performed on the R-1, R-2, and R-3 samples. The rutile phase was identified from the powder x-ray diffraction patterns of all three specimens (Fig. 7). Compared to the mineral phase constitution of Brahmaputra River basin ilmenite concentrate (Fig. 4), the prepared products show new diffraction peaks of rutile, indicating ilmenite dissolution occurs. However, the peak intensity was comparatively higher in the R-2 sample than others, which in turn indicated the better crystallinity of R-2 (Fig. 7). Besides, similarities in the XRD pattern

Table II. Chemical composition of the prepared titanium product and other synthetic rutile

Oxides (wt.%)	Titanium products from Brahmaputra River basin ilmenite concentrate			Synthetic rutile from Tronox, Western Australia ^{20,50}	Synthetic rutile from Rosetta beach ilmenite, Egypt ¹⁰	Synthetic rutile from beach ilmenite of Murray Basin, Australia ⁴⁶	Synthetic rutile nanoparticles from ilmenite ore of Abu Ghalaga, Egypt ²⁷
	R-1	R-2	R-3				
Al ₂ O ₃	0.07	–	0.20	1.10	0.44	0.13	0.10
SiO ₂	0.12	0.20	0.17	0.79	1.50	0.79	3.20
P ₂ O ₅	0.12	0.17	0.12	0.02	–	0.02	–
CaO	0.06	0.03	0.07	0.04	–	0.01	–
TiO ₂	86.27	95.61	90.14	92.00	89.00	97.30	95.92
Cr ₂ O ₃	–	–	–	0.13	0.175	0.02	–
MnO	–	–	–	0.73	0.45	0.01	–
Fe ₂ O ₃ ^t	13.19	3.81	9.20	3.20	6.70	1.08	0.42
MgO	–	–	–	0.33	–	0.02	0.35
Nb ₂ O ₅	0.12	0.15	0.08	0.22	–	0.23	–
V ₂ O ₅	–	–	–	0.32	0.064	0.02	–

^tFe₂O₃^t = Total of FeO + Fe₂O₃.

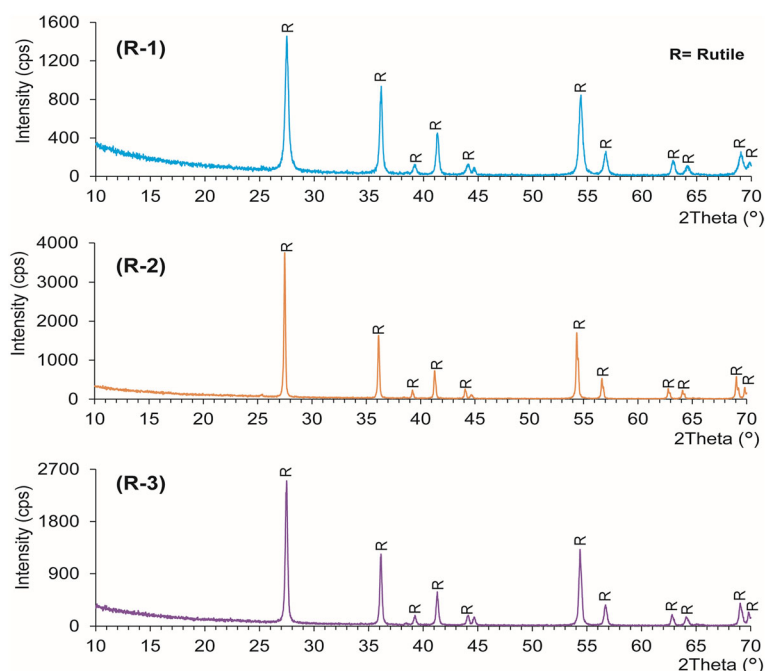


Fig. 7. XRD pattern of prepared titanium products (R-1, R-2, and R-3 samples).

were observed between the experimental data and the standard ICDD database (#00-021-1276) in terms of peak position and relative intensity of the rutile phase. From the discussion of XRD data, the prepared titanium product is fully composed of the rutile phase; here it can be designated as synthetic rutile. Thus, the prepared synthetic rutile of R-2, i.e., the synthesizing product using concentrated HCl with an acid-to-ilmenite ratio of 5:1 at $75 \pm 5^\circ\text{C}$ for 3 h at a stirring speed of 250 rpm, provides an excellent product with higher crystallinity than others.

Phase purity is crucial when producing synthetic rutile for various applications. For further confirmation of the phase purity of rutile as evident from the XRD result (Fig. 7), a complementary Raman spectroscopic analysis on an unoriented sample using 785 nm laser light has been accomplished (Fig. 8). It also provides additional evidence of the presence of rutile and the absence of other phases. The Raman spectrum was similar to the rutile phases as obtained from characteristic stretching peaks at 247.56 cm^{-1} , 445.93 cm^{-1} , and 609.69 cm^{-1} . The presence of these distinct Raman peaks confirms that the product is entirely composed of synthetic rutile. Furthermore, comparable Raman peaks (wave numbers) were found in published articles.^{51,52} The complementary Raman spectroscopic analysis supports and further confirms the synthetic rutile phase purity, as indicated by the presence of characteristic stretching peaks that are consistent with the synthetic rutile phase.

The morphology and physical structure of prepared synthetic rutile were evaluated using a *Zeiss Sigma 300* FESEM, where magnification was 10 K

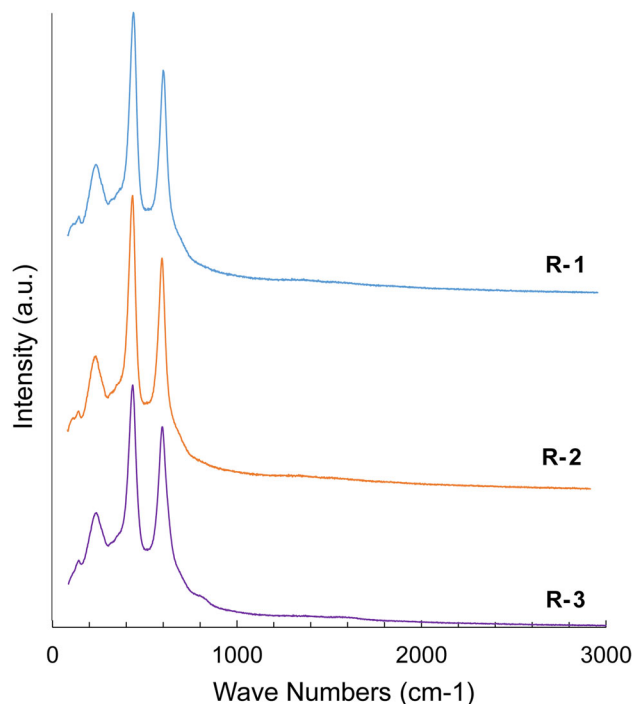


Fig. 8. Raman spectra of R-1, R-2, and R-3 samples.

(Fig. 9). The synthetic rutile (TiO_2) has clusters of spherical crystallites in samples of R-1 and R-3 but a crushed appearance of crystallites in samples of R-2. The approximate diameter (average size) of particles in the R-1, R-2, and R-3 specimens was < 2 , < 0.5 , and $< 3\ \mu\text{m}$, respectively (Fig. 9). In addition, the back-scattered electron (BSE) image showed that the R-2 specimen was more porous

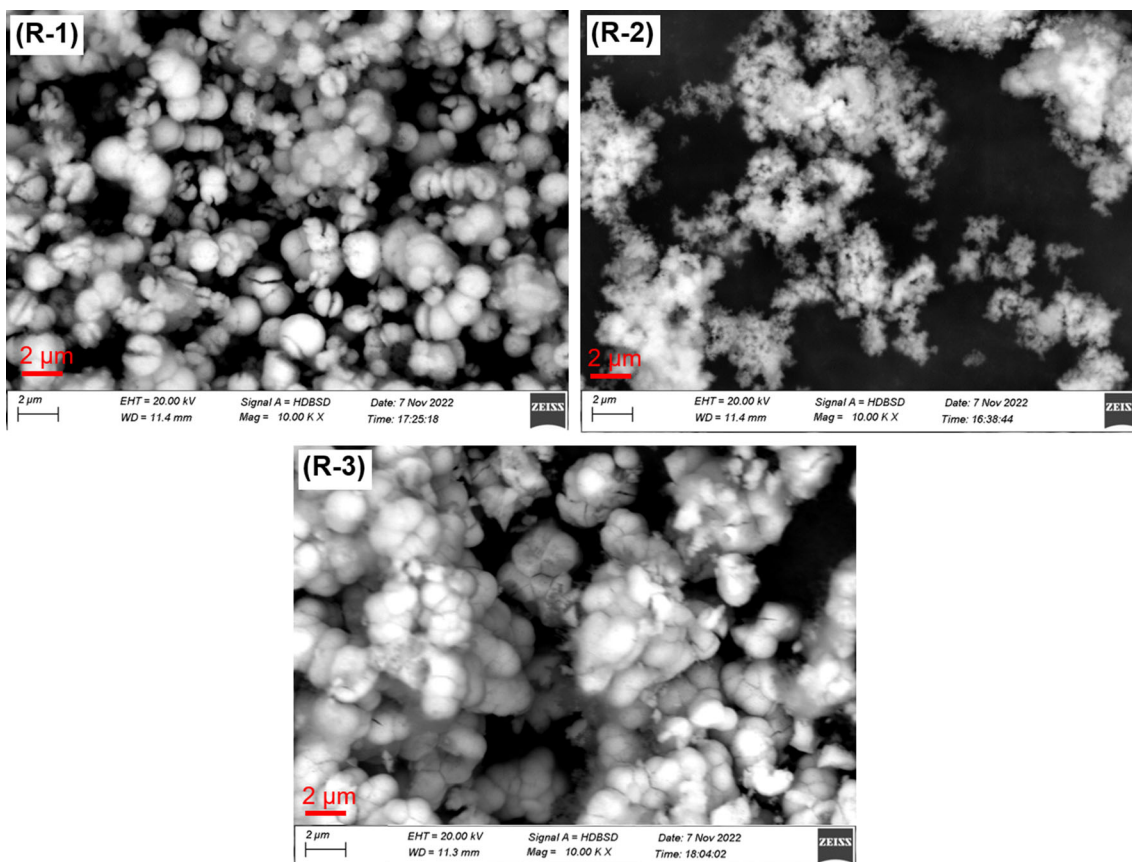


Fig. 9. Back-scattered electron (BSE) images of upgraded products of synthetic rutile.

than those of the R-1 and R-3 specimens. Based on the findings of the chemical composition, XRD and Raman spectra, and BSE image, it was clear that the R-2 specimen outperformed the R-1 and R-3 specimens. Accordingly, the characteristics of the R-2 product obtained from the BSE microphotograph combined with the chemical and spectroscopic analyses suggest that the leaching conditions for the R-2 sample were favorable for synthetic rutile extraction.

Based on the aforementioned chemical framework, diffraction pattern, Raman, and FESEM analysis, the features of the R-2 product are superior to those of R-1 and R-3 for the manufacturing of TiO_2 pigments. The R-2 product has a TiO_2 purity of 95.61% (Table II) and shows a comparatively higher peak intensity (Fig. 7), which implies better crystallinity than R-1 and R-3 and represents an absolutely synthetic rutile phase (Figs. 7 and 8). This R-2 synthetic rutile is porous and has a crushed appearance of crystallites, with a particle size of $< 0.5 \mu\text{m}$ (Fig. 9). These properties suggest that the hydrometallurgical criteria of R-2 are beneficial for synthetic rutile preparation, employing concentrated HCl with an acid-to-ilmenite ratio of 5:1 at $75 \pm 5^\circ\text{C}$ for 3 h at a stirring speed of 250 rpm. It can also be concluded that the procedure consisting of mechanical activation of ilmenite

concentrate, acid leaching, boiling, filtration, and calcination was an effective way to produce synthetic rutile (Fig. 2). However, to understand the dissolution efficiencies of Brahmaputra River basin ilmenite in HCl acid solutions, a further investigation of leaching kinetics is required.

Industrial Prospect

The best titanium-based product (R-2) prepared in this study is entirely synthetic rutile with a purity of 95.61% TiO_2 . The only coloring compound, iron oxides (3.81%), is present in the prepared porous synthetic rutile (Table II), which can be removed by chlorination. The other coloring metals, MnO and Cr_2O_3 , were not found. The amount of other oxides of Si, P, Ca, and Nb is very negligible, while Cr and V are not detected in the extracted synthetic rutile (R-2). The chemical data described here are acceptable and meet the industrial specification for the production of white pigment, with the slight exception of the presence of iron oxides (Fe_2O_3 3.81%), which can be reduced by the chlorination process.^{20,27,49,53} In addition, the chemical composition of synthetic rutile (R-2) produced from Brahmaputra River basin ilmenite is comparable to the synthetic rutile of Tronox, Western Australia (Table II), indicating the products have industrial applications.

CONCLUSION

The synthetic rutile preparation from river basin ilmenite is a relatively untouched research area compared to beach placer ilmenite or massive crystalline ore bodies. In this study, fluvial Brahmaputra River basin ilmenite concentrate has been characterized, and simultaneously, attempts have been made to produce synthetic rutile via direct HCl acid leaching of a potential alternative source of river basin ilmenite feed. The following findings were obtained:

- Chemically, the ilmenite concentrate consists of 27.02% TiO₂ with impurities of 60.62% Fe₂O₃^t and 12.36% oxides of Si, Al, Ca, Mg, P, Cr, Mn, and Nb. The content of impurities is higher than that of equivalent beach placer ilmenite or crystalline ilmenite ore, making them low grade. Mineralogically, it comprises primarily ilmenite phases with less hematite, minor quartz, and rutile, indicating a lower degree of liberation, chemical weathering, sorting, reworking, etc. The ilmenite grain has a sub-angular to sub-rounded shape with an average size of 168 μm, while mechanical activation reduces the mean size to 20.09 μm. The texture of ilmenite showed the presence of liberated ilmenite grains, exsolution of hemo-ilmenite and ilmeno-hematite, and some locked grains of gangue minerals as inclusions.
- Upgrading attempts of ilmenite to titanium products showed the prepared highest purity product (R-2) from the hydrometallurgical route was entirely composed of the synthetic rutile (TiO₂) phase, which contains 95.61% TiO₂ and 3.81% Fe₂O₃^t with traces of other oxides (0.58%). The only coloring agent (Fe₂O₃) might be removed by the selective chlorination process. The crystallite size of the porous synthetic rutile (R-2) was < 0.5 μm obtained from a BSE microphotograph. The chemistry, phase purity, and morphology suggest that the present river basin ilmenite is a promising new feedstock for synthetic rutile preparation by direct HCl acid leaching. The favorable condition for the two-step leaching was an acid-to-ilmenite ratio of 5:1 at 75 ± 5°C for 3 h at a stirring speed of 250 rpm using concentrated HCl acid.
- The TiO₂ purity and sum of other associated oxides, excluding iron oxide (3.81% Fe₂O₃^t) in the synthetic rutile, indicate its suitability for industrial use. This iron oxide content can be minimized by chlorination. The prepared synthetic rutile (TiO₂) could be used in various industries, e.g., paint, plastic, welding electrodes, coatings, paper, etc. Finally, this research gives a new understanding of the utilization of river basin ilmenite feedstock for synthetic rutile production.

ACKNOWLEDGEMENTS

The authors are grateful to the authority of the Bangladesh Council of Scientific and Industrial Research (BCSIR) for approving the R&D work (Ref. No.: 39.02.0000.011.14.111.2019/224, Date: 07.11.2019, R&D Project ID: 54, FY: 2019-2020). We thank Mr. A.S.M. Mehedi Hasan for his assistance during the FESEM study. The authors also acknowledged the handling editor and anonymous reviewers for their helpful assistance and comments to improve the manuscript.

AUTHOR CONTRIBUTIONS

MSR: Conceptualization, methodology, designing and conducting experiments, data analysis, writing original draft. MSS: Methodology, designing experiments, conducting experiment. PKB: Conceptualization, supervision, review. MSS: Conducting experiments, review, editing. FA: Formal analysis, review, editing. MNZ: Review revised manuscript, supervision. All authors read and approved the final manuscript.

FUNDING

This research is funded by the Bangladesh Council of Scientific and Industrial Research (BCSIR) through an annual R&D project.

CONFLICT OF INTEREST

The authors declare that they have no conflict of interest.

REFERENCES

1. M.J. Gázquez, J.P. Bolívar, R. García-Tenorio, and F. Vaca, *Mater. Sci. Appl.* <https://doi.org/10.4236/msa.2014.57048> (2014).
2. T.H. Nguyen and M.S. Lee, *Miner. Process. Extr. Metall. Rev.* <https://doi.org/10.1080/08827508.2018.1502668> (2019).
3. J. Xiang, G. Pei, W. Lv, S. Liu, X. Lv, and G. Qiu, *Chem. Eng. Process. Process Intensif.* <https://doi.org/10.1016/j.cep.2019.107774> (2020).
4. N. El-Hazek, T.A. Lasheen, R. El-Sheikh, and S.A. Zaki, *Hydrometallurgy.* <https://doi.org/10.1016/j.hydromet.2007.01.003> (2007).
5. W. Spencer, D. Ibana, P. Singh, and A.N. Nikoloski, *Miner. Eng.* <https://doi.org/10.1016/j.mineng.2021.107365> (2022).
6. W. Zhang, Z. Zhu, and C.Y. Cheng, *Hydrometallurgy.* <https://doi.org/10.1016/j.hydromet.2011.04.005> (2011).
7. USGS, Mineral commodity summaries 2023: titanium mineral concentrates. U.S. Geological Survey, Reston, Virginia, USA (2023). <https://doi.org/10.3133/mcs2023>.
8. M. Hope, Mineral sand price forecasts. Diversified Metals & Mining, Asia Pacific/Australia (2016).
9. F. Habashi, F. Kamaliddine, and E. Bourricaudy, in A new process to upgrade ilmenite to synthetic rutile, *Conference of Metallurgists Proceedings 2014, Canadian Institute of Mining, Metallurgy and Petroleum, Vancouver* (2014).
10. T.A.I. Lasheen, *Hydrometallurgy.* <https://doi.org/10.1016/j.hydromet.2004.10.002> (2005).
11. C. Li, B. Liang, and H. Wang, *Hydrometallurgy.* <https://doi.org/10.1016/j.hydromet.2007.11.013> (2008).
12. M.H.H. Mahmoud, A.A.I. Afifi, and I.A. Ibrahim, *Hydrometallurgy.* <https://doi.org/10.1016/j.hydromet.2003.08.001> (2004).

13. K.J. Stanaway, *Min. Eng.* 46, 1367 (1994).
14. A. Mehdilo and M. Irannajad, *Arab. J. Geosci.* <https://doi.org/10.1007/s12517-012-0647-x> (2013).
15. M.K. Sarker, A.K.M.B. Rashid, and A.S.W. Kurny, *Intl. J. Miner. Process.* <https://doi.org/10.1016/j.minpro.2006.04.005> (2006).
16. C. Sasikumar, D.S. Rao, S. Srikanth, B. Ravikumar, N.K. Mukhopadhyay, and S.P. Mehrotra, *Hydrometallurgy.* <http://doi.org/10.1016/j.hydromet.2004.08.001> (2004).
17. A.S.M.A. Haseeb, M.Z. Huq, and A.S.W. Kurny, *Transact. Inst. Min. Metall. Sect. C* 106, 39–43 (1997).
18. N.N. Shams and A.S.W. Kurny, in Effects of catalysis on the extent of reduction of Bangladesh ilmenite, *Proceedings of the Mineral Processing Waste and Environment Management, New Delhi* (2000), pp. 271–276.
19. A. Rahman, J. Tardio, S.K. Bhargava, M.N. Zaman, A.S.M.M. Hasan, A. Torpy, and M.I. Pownceby, *Ore Geol. Rev.* <https://doi.org/10.1016/j.oregeorev.2019.103271> (2020).
20. D. Filippou and G. Hudon, Minerals, Slags, and Other Feedstock for the Production of Titanium Metal, in *Extractive Metallurgy of Titanium*. (Elsevier, 2020).
21. R. Vasquez and A. Molina, in Leaching of ilmenite and pre-oxidized ilmenite in hydrochloric acid to obtain high grade titanium dioxide, *Proceedings of the 17th International Metallurgical & Materials Conference Proceedings: METAL, Hradec and Moravici, Czech Republic, 13–15 May* (2008).
22. C. Li, B. Liang, L. Guo, and Z. Wu, *Miner. Eng.* <https://doi.org/10.1016/j.mineng.2006.02.005> (2006).
23. C. Li, B. Liang, and L. Guo, *Hydrometallurgy.* <https://doi.org/10.1016/j.hydromet.2007.04.002> (2007).
24. C. Sasikumar, D.S. Rao, S. Srikanth, N.K. Mukhopadhyay, and S.P. Mehrotra, *Hydrometallurgy.* <https://doi.org/10.1016/j.hydromet.2007.03.013> (2007).
25. N.J. Welham and D.J. Llewellyn, *Miner. Eng.* [https://doi.org/10.1016/S0892-6875\(98\)00070-3](https://doi.org/10.1016/S0892-6875(98)00070-3) (1998).
26. W.J. Bruckard, M.I. Pownceby, L.K. Smith, and G.J. Sparrow, *Miner. Process. Extr. Metall.* <https://doi.org/10.1179/1743285514Y.0000000083> (2015).
27. M.G. Shahien, M.M. Khedr, A.E. Maurice, A.A. Farghali, and R.A. Ali, *Beni Suef Univ. J. Basic Appl. Sci.* <https://doi.org/10.1016/j.bjbas.2015.05.013> (2015).
28. A. Rahman, M.I. Pownceby, J. Tardio, G.J. Sparrow, N. Haque, and F. Hasan, *Minerals.* <https://doi.org/10.3390/min11070786> (2021).
29. J. Akter, D. Roelvink, and M. van der Wegen, *Estuar. Coast. Shelf Sci.* <https://doi.org/10.1016/j.ecss.2021.107509> (2021).
30. M. Rahman, M. Dustegir, R. Karim, A. Haque, R.J. Nicholls, S.E. Darby, H. Nakagawa, M. Hossain, F.E. Dunn, and M. Akter, *Sci. Total. Environ.* <https://doi.org/10.1016/j.scitotenv.2018.06.147> (2018).
31. P.K. Biswas, S.S. Ahmed, M.I. Pownceby, N. Haque, S. Alam, M.N. Zaman, and M.A. Rahman, *Appl. Earth Sci.* <https://doi.org/10.1080/25726838.2018.1488357> (2018).
32. D.K. Datta and V. Subramanian, *Environ. Geol.* <https://doi.org/10.1007/s002540050145> (1997).
33. M.J.J. Rahman, M.I. Pownceby, and M.S. Rana, *Ore Geol. Rev.* <https://doi.org/10.1016/j.oregeorev.2022.104773> (2022).
34. S.K. Singh and C. France-Lanord, *Earth Planet. Sci. Lett.* [https://doi.org/10.1016/S0012-821X\(02\)00822-1](https://doi.org/10.1016/S0012-821X(02)00822-1) (2002).
35. V.N. Mikhailov and M.A. Dotsenko, *Water Resour.* <https://doi.org/10.1134/S0097807806040014> (2006).
36. M. Kumar, V. Srivastava, P. Mazumder, J.P. Deka, S. Gupta, R. Goswami, P.K. Mutiyar, S. Dave, C. Mahanta, A.L. Ramanathan, and M. Joshi, *Environ. Res.* <https://doi.org/10.1016/j.envres.2021.112067> (2022).
37. J.M. Coleman, *Sediment. Geol.* [https://doi.org/10.1016/0037-0738\(69\)90010-4](https://doi.org/10.1016/0037-0738(69)90010-4) (1969).
38. M.S. Hossain, M.T. Aziz, M.S. Shahriar, and A.A. Ritu, *J. Geol. Soc. India.* <https://doi.org/10.1007/s12594-021-1713-3> (2021).
39. M.A. Rahman, M.I. Pownceby, N. Haque, W.J. Bruckard, and M.N. Zaman, *Appl. Earth Sci.* <https://doi.org/10.1080/03717453.2015.1115159> (2016).
40. B.A. Wills and J.A. Finch, Magnetic and Electrical Separation, in *Wills' Mineral Processing Technology*. (Elsevier, 2016), pp. 381–407.
41. K. Norrish and J.T. Hutton, *Geochim. Cosmochim. Acta.* [https://doi.org/10.1016/0016-7037\(69\)90126-4](https://doi.org/10.1016/0016-7037(69)90126-4) (1969).
42. R.C. Lindholm, *Mineral Identification Using X-ray Diffraction BT—A Practical Approach to Sedimentology* (Springer Netherlands, 1987).
43. ASTM-D422, Standard Test Method for Particle-Size Analysis of Soils (2007). <https://doi.org/10.1520/D0422-63R07E02>.
44. R.G. Haverkamp, D. Kruger, and R. Rajashekar, *Hydrometallurgy.* <https://doi.org/10.1016/j.hydromet.2016.04.015> (2016).
45. I. Grey, C. MacRae, E. Silvester, and J. Susini, *Mineral. Mag.* <https://doi.org/10.1180/0026461056940261> (2005).
46. E.A. Walpole and J.D. Winter, *The Austpac ERMS and EARS processes for the manufacture of high-grade synthetic rutile by the hydrochloric acid leaching of ilmenite*, ed E. Peek, G. Van Weert. Chloride metallurgy, vol 2 (Metallurgical Society of the Canadian Institute of Mining, Metallurgy and Petroleum, Montreal, 2002), pp. 401–415.
47. ASTM-D2487, Standard Practice for Classification of Soils for Engineering Purposes (Unified Soil Classification System) (2017). <https://doi.org/10.1520/D2487-17>.
48. A.S.M.M. Hasan, I. Hossain, M.A. Rahman, M.S. Rahman, M.N. Zaman, and P.K. Biswas, *Arab. J. Geosci.* <https://doi.org/10.1007/s12517-018-3905-8> (2018).
49. E.J. Jung, J. Kim, and Y.R. Lee, *Sci. Rep.* <https://doi.org/10.1038/s41598-021-83485-6> (2021).
50. Mineral Sands Annual Review, TZ Mineral International Pty Ltd., Victoria Park, Western Australia (2011).
51. S. Challagulla, K. Tarafder, R. Ganesan, and S. Roy, *Sci. Rep.* <https://doi.org/10.1038/s41598-017-08599-2> (2017).
52. V. Tamilselvan, D. Yuvaraj, R.R. Kumar, and K.N. Rao, *Appl. Surf. Sci.* <https://doi.org/10.1016/j.apsusc.2011.12.079> (2012).
53. J.A. Kahn, *J. Miner. Met. Mater. Soc.* <https://doi.org/10.1007/BF03338498> (1984).

Publisher's Note Springer Nature remains neutral with regard to jurisdictional claims in published maps and institutional affiliations.

Springer Nature or its licensor (e.g. a society or other partner) holds exclusive rights to this article under a publishing agreement with the author(s) or other rightsholder(s); author self-archiving of the accepted manuscript version of this article is solely governed by the terms of such publishing agreement and applicable law.